Growth Mechanism of Catalyst-Free and Mask-Free Heteroepitaxial GaN Submicrometer- and Micrometer-Sized Rods under Biaxial Strain: Variation of Surface Energy and Adatom Kinetics

ARTICLE *in* CRYSTAL GROWTH & DESIGN · AUGUST 2012

Impact Factor: 4.89 · DOI: 10.1021/cg300764f

8 AUTHORS, INCLUDING:

Suk-Min Ko
Korea Advanced Institute of Science and Tech…
17 PUBLICATIONS **81** CITATIONS
SEE PROFILE

Young-Ho Ko
Electronics and Telecommunications Researc…
13 PUBLICATIONS **69** CITATIONS
SEE PROFILE

Yong-Hyun Kim
Korea Advanced Institute of Science and Tech…
106 PUBLICATIONS **2,889** CITATIONS
SEE PROFILE

CRYSTAL GROWTH & DESIGN

Communication

pubs.acs.org/crystal

Growth Mechanism of Catalyst-Free and Mask-Free Heteroepitaxial GaN Submicrometer- and Micrometer-Sized Rods under Biaxial Strain: Variation of Surface Energy and Adatom Kinetics

Suk-Min Ko,[†] Je-Hyung Kim,[†] Young-Ho Ko,[†] Yun Hee Chang,[‡] Yong-Hyun Kim,[‡] Jongmoon Yoon,[§] Jeong Yong Lee,[§] and Yong-Hoon Cho*,[†]

[†]Department of Physics and Graduate School of Nanoscience & Technology (WCU), Korea Advanced Institute of Science and Technology (KAIST), Daejeon 305-701, The Republic of Korea

[‡]Graduate School of Nanoscience and Technology (WCU), KAIST, Daejeon 305-701, The Republic of Korea

[§]Department of Materials Science and Engineering, KAIST, Daejeon 305-701, The Republic of Korea

Supporting Information

ABSTRACT: We report the formation mechanism and the characteristics of catalyst-free and mask-free heteroepitaxial GaN submicrometer- and micrometer-sized rods (SMRs) under biaxial strain grown on Si(111) substrates by metal−organic chemical vapor deposition. We found that the GaN SMRs on Si(111) substrates were subject to strong tensile strain on their N-terminated top $(000\bar{1})$ GaN surface due to the lattice mismatch between GaN and Si. Our calculations based on the density functional theory showed that the $(000\bar{1})$ GaN surface energy increased (decreased) monotonically with increasing tensile (compressive) strain, resulting in a faster GaN growth rate of the tensile-strained top $(000\bar{1})$ surface of GaN SMRs than that of the compressive-strained one. We experimentally verified this result by comparing GaN on Si(111) substrates with tensile strain and on 6H-SiC substrates with compressive strain. In addition, we confirmed that the vertical growth rate of GaN SMRs could be controlled by adjusting growth conditions, especially the reactor pressures at low V/III molar ratio. We explained the changes in the growth rate by introducing the pressure dependency of the reaction rate constant, the chemical potential, and the surface diffusion length of Ga adatom on the surface of the SMRs.

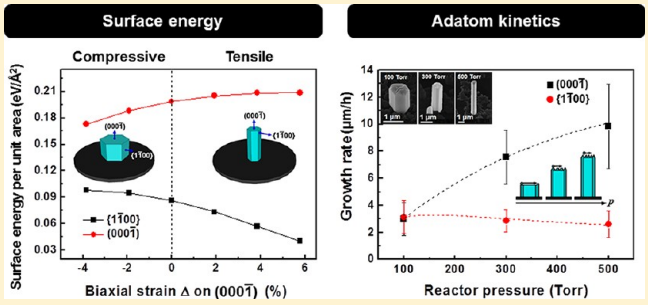

1. INTRODUCTION

GaN submicrometer- and micrometer-sized rods (SMRs) are some of the most promising structures for high performance optoelectronic devices, such as light emitting diodes (LEDs),[1,2] lasers,[3,4] and solar cells,[5] due to their high quantum efficiency and high surface to volume ratio. However, it is not easy to grow GaN SMRs with a high aspect ratio without the assistance of a metal catalyst,[6,7] a patterning mask,[1,8,9] or a doping constituent, as a result of the long lateral diffusion length of adatom on the top surface of GaN that leads to the energetically favored thermodynamic equilibrium shape, especially at the high growth temperatures (>1000 °C) and the high V/III precursor molar ratio of metal−organic chemical vapor deposition (MOCVD), contrary to molecular beam epitaxy[5,10,11] or hydride vapor phase epitaxy,[12] which can grow the vertically well-oriented GaN SMRs without difficulties. Nevertheless, in the case of the vapor−liquid−solid (VLS), metal catalysts, such as Au or Ni, may act as impurities and GaN SMRs produced in this manner are not vertically aligned well. Moreover, the selective area growth technique with the patterning mask generally includes complex and expensive processes, and the quality and the polarity of the grown SMRs were strongly determined by the GaN template below the pattern. Recently, only a few studies have reported GaN SMRs grown by MOCVD under different growth conditions and substrates. However, the detailed atomistic formation kinetics or growth mechanisms for the GaN SMRs are not yet clearly understood.

In this paper, we demonstrate the strong influence of biaxial strain that acts as a driving force on the growth mechanism of vertically well-aligned GaN SMRs on Si(111) substrates without the use of metal catalysts or masks. The density functional theory (DFT) was employed to verify the effect of biaxial strain on GaN SMRs. We also investigated the correlation between the reactor pressure and the growth rate of the SMRs as well as the influence of biaxial strain on GaN SMRs growth on Si(111) and 6H-SiC substrates for comparison. We found that the surface morphologies of the GaN SMRs could be strongly influenced by (i) the reaction rate constant corresponding to the reactor pressure during growth, (ii) the variation on the diffusion barrier due to the biaxial

Received: June 4, 2012
Published: July 10, 2012

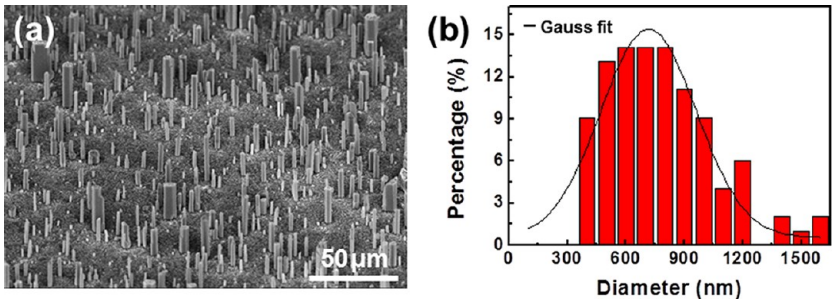

Figure 1. (a) Bird's-eye-view SEM image of GaN SMRs grown at 500 Torr. (b) Distribution in diameter of the GaN SMRs.

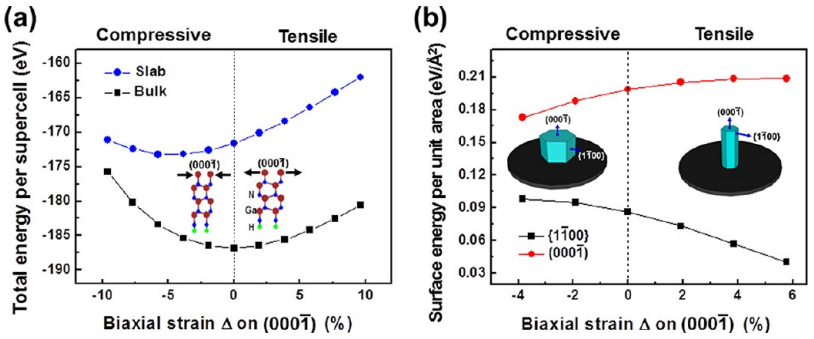

Figure 2. (a) Calculated slab and bulk energies of a GaN supercell for the (000$\bar{1}$) plane. (b) Surface energies per unit cell of the {1$\bar{1}$00} and the (000$\bar{1}$) planes with the various biaxial strains on the (000$\bar{1}$) plane.

strain, and (iii) the change in the surface energy due to the biaxial strain. From the results, we could successfully explain the growth mechanism of catalyst-free and mask-free heteroepitaxial GaN SMRs on the Si(111) substrate.

2. EXPERIMENTAL SECTION

2.1. Growth Procedure. GaN submicrometer- and micrometer-sized rods (SMRs) were grown on Si(111) substrates by using MOCVD (Sysnex Marvel 260 NT). As the group III and V precursors, trimethylgallium (TMGa) and NH_3 were used. N_2 and H_2 gases were used as the carrier gas during the growth. The Si(111) substrates were cleaned in a mixture of H_2SO_4 and deionized water (10:1) at room temperature for 15 min and were rinsed in deionized water. Two-inch Si(111) substrates were mounted onto a six-pocket susceptor in the reaction chamber. 6H-SiC substrates were also used for comparison to confirm the strain effect. Initially, the Si(111) and the 6H-SiC substrates were thermally etched to remove the natural oxide layer at 1140 °C in a H_2 ambient for 10 min. To prevent the formation of a SiN_x layer by nitridation, TMGa was spread onto the surface of the substrates without NH_3 for 20 s. Then, GaN was directly deposited on the Si(111) substrate at high growth temperature (1000 °C) by a two-step process without a buffer layer. First, GaN was grown in the N_2 ambient to form GaN islands and to coalesce them. Next, the growth atmosphere was changed from a N_2 ambient to a H_2 ambient to etch the residual GaN islands from the surface of the substrate except for GaN SMRs. During the GaN growth, we kept the NH_3 flux stable while the flow rate of the TMGa was periodically changed to control the shape and the growth mode of the GaN SMRs. To increase the vertical growth rate, we reduced the V/III molar ratio from 1780.9 to 66.7 and raised the reactor pressure from 100 to 500 Torr.

2.2. Characterization. The structural properties of GaN SMRs were investigated by scanning electron microscopy (SEM, Hitachi s-4800) and transmission electron microscopy (TEM, Jeol 3010). The optical properties of a single GaN SMR were investigated by cathodoluminescence (CL, Gatan mono CL 4) experiments at room temperature.

2.3. Simulation Methodology. The surface energy of strained (000$\bar{1}$) and {1$\bar{1}$00} GaN surfaces was calculated with the first-principles total energy calculation method using plane waves and DFT formulations as implanted in the Vienna Ab initio Simulation Package.[13] The kinetic energy cutoff of plane waves was 400 eV. The projected augmented wave potentials[14] and the Perdew–Burke–Ernzerh[15] exchange-correlation functional were used for the surface energy calculations of the (000$\bar{1}$) and the {1$\bar{1}$00} GaN planes. To simulate the (000$\bar{1}$) GaN surface with N-polarity, we used a slab model of four GaN double layers and 10 Å vacuum layers with the back-surface passivated by 1.25 pseudo-hydrogen and a bulk of four GaN double layers. The same values of lattice constants a and c were used for the strained {1$\bar{1}$00} GaN surface, just as for the (000$\bar{1}$) GaN plane. The cell of {1$\bar{1}$00} GaN that does not have polarity was designed without pseudo-hydrogen passivation. The atomic structures for the surface energy calculation of the (000$\bar{1}$) and the {1$\bar{1}$00} GaN planes are described in the Supporting Information. The 4 × 4 × 1 and 4 × 4 × 4 k-points with a sampling the Γ-point were used for the Brillouin zone integration of the slab and the bulk of the (000$\bar{1}$) GaN plane. 8 × 8 × 4 and 8 × 8 × 1 k-points sampling for the bulk and the slab energies were used for the strained {1$\bar{1}$00} GaN surface.

3. RESULTS AND DISCUSSION

Figure 1a shows the 30-deg-tilted SEM images of the SMRs grown under 500 Torr for 20 min. The GaN SMRs are uniformly located and vertically well aligned on the Si(111) substrate. We obtained the heteroepitaxial SMRs with high aspect ratios directly grown on Si(111) substrates by using only Ga and N precursors without any metal-catalyst or patterned mask or doping constituents. Figure 1b shows the distributions in diameter of the GaN SMRs. The density of the GaN SMRs is about 2.44 × 10^6 cm^{-2}. The average diameter of the GaN SMRs is about 865 ± 33 nm, and their mean length is about 3.29 ± 1.04 μm. The variations in diameter occur due to the weak driving force in our self-assembled growth method compared to the catalyst-assisted vapor–liquid–solid growth method[6,7] or template-directed synthesis,[16] which leads to severe anisotropic growth with a tremendous difference in the

dx.doi.org/10.1021/cg300764f | Cryst. Growth Des. 2012, 12, 3838–3844

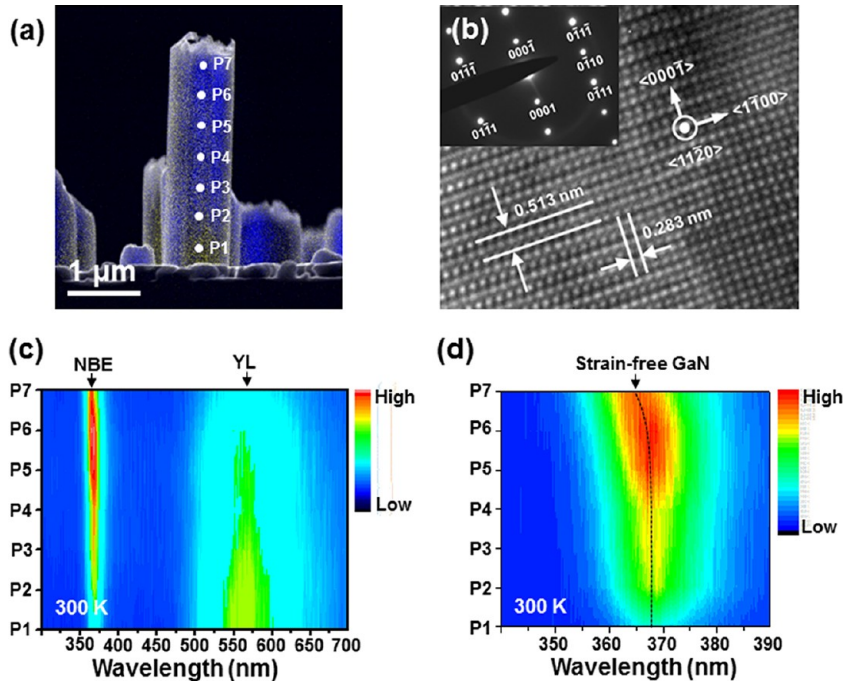

Figure 3. (a) Monochromatic CL images (blue and yellow indicate NBE and YL, respectively) of GaN single SMR with an SEM image. (b) High-resolution TEM lattice images and a diffraction pattern of GaN SMR taken along the [11$\bar{2}$0] zone-axis (inset). (c) CL spectra from different positions (P1 to P7). (d) CL spectra measured around the NBE peak of GaN.

surface energies between the growth direction of ⟨000$\bar{1}$⟩ and its perpendicular direction of [1$\bar{1}$00].

If the effects of the adatom kinetics by the variation of growth conditions are not considered, the thermodynamic equilibrium shape is then determined only by the difference of the surface energy of each crystal plane on GaN SMRs.[17,18] Generally, GaN SMRs on Si(111) substrate have N-polarity with two crystal planes, i.e., a top (000$\bar{1}$) GaN surface and {1$\bar{1}$00} GaN sidewalls, since the surface energies of the top (000$\bar{1}$) GaN surface and the {1$\bar{1}$00} GaN sidewalls are lower than those of the other crystallographic planes.[19] We expected that the surface energy difference between the top (000$\bar{1}$) GaN surface and the {1$\bar{1}$00} GaN sidewalls plays a crucial role in determining the shape of GaN SMRs and that the surface energies of the top (000$\bar{1}$) GaN surface and {1$\bar{1}$00} GaN sidewall are influenced by biaxial strain. To confirm the influence of the biaxial strain on the surface energy difference between the top (000$\bar{1}$) GaN surface and the {1$\bar{1}$00} GaN sidewalls, the total energies of slab and bulk of GaN were calculated at the various biaxially strained conditions by DFT simulation. Figure 2a shows the calculated total energies of the strained slab and bulk for the top (000$\bar{1}$) GaN surface, $E_{Slab}^{(000\bar{1})}(\Delta)$ and $E_{Bulk}^{(000\bar{1})}(\Delta)$, as a function of the biaxial strain Δ on the (000$\bar{1}$) GaN surface up to ±10%. The total energy of the slab for the top (000$\bar{1}$) GaN surface is higher than that of bulk, as expected, but the minimum total energy of slab occurs at a compressive strain region (Δ = −6%). Because of the difference between the total energy minima of the slab and of the bulk for the top (000$\bar{1}$) GaN surface, the surface energy, i.e., $E_{Slab}^{(000\bar{1})}(\Delta) - E_{Bulk}^{(000\bar{1})}(\Delta)$, monotonically varies within the range of Δ = ±10%; the tensile strain causes higher surface energy on the top (000$\bar{1}$) GaN surface than does the compressive strain. Figure 2b shows the surface energy per unit area (eV/Å^2) for the top (000$\bar{1}$) GaN surface and {1$\bar{1}$00} GaN sidewalls. The surface energy per unit area for the top (000$\bar{1}$) GaN surface reaches its maximum at Δ = 4%, whereas that for the {1$\bar{1}$00} GaN sidewalls gradually decreases in the tensile strain region. Therefore, the surface energy difference between the top (000$\bar{1}$) GaN and the {1$\bar{1}$00} GaN sidewalls increases in the tensile strain region. This theoretical result explains why we were able to achieve a higher aspect ratio of GaN SMRs on the Si(111) surface. In order to verify the strain effect experimentally, we tried to grow the GaN SMRs simultaneously on 6H-SiC and Si(111) substrates, which provide different biaxial strains on the top (000$\bar{1}$) surface of the GaN SMRs. The top (000$\bar{1}$) surface of GaN SMRs on the Si(111) substrate undergoes a strong tensile strain of 16.36%, whereas that of GaN structures (i.e., microplates) on the 6H-SiC substrate suffers a weak compressive strain of 4.55% at the growth temperature (1000 °C).[20−22] This experimental result strongly supports that if the surface energy difference between the top (000$\bar{1}$) surface and the {1$\bar{1}$00} sidewalls increased remarkably due to tensile strain [e.g., in the case of GaN grown on the Si(111) substrate], the GaN could grow much faster in the direction of the (000$\bar{1}$) plane to finally form GaN SMRs.

We carried out CL and TEM experiments to investigate the magnitude of biaxial strain on different positions in the GaN SMR along the growth axis of ⟨000$\bar{1}$⟩. Figure 3a shows a superimposed image of monochromatic CL images of a single GaN SMR taken at 365 and 566 nm together with the SEM image at room temperature. Blue represents the GaN near-band-edge (NBE) emission, and yellow represents the yellow luminescence (YL). The upper side of the GaN SMR radiates strong NBE emission at about 365 nm with weak YL, while the lower side shows weak NBE emission with distinct YL at around 566 nm, indicating that the crystalline quality in the upper area is better than that in the lower area. There are two possible reasons for these results. First, the bottom of the GaN SMRs may have some defects or dislocations due to the direct growth on the Si(111) substrate without any buffer layer.[23,24]

dx.doi.org/10.1021/cg300764f | Cryst. Growth Des. 2012, 12, 3838−3844

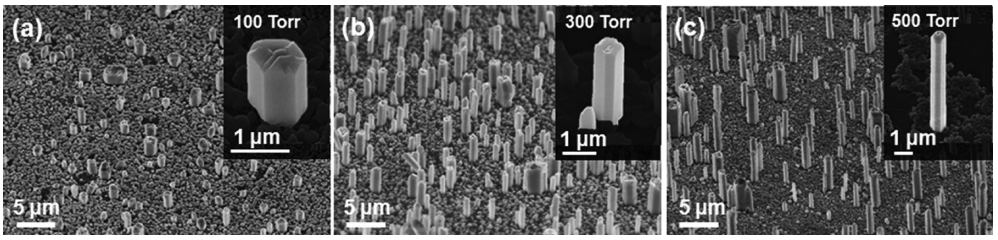

Figure 4. SEM images of GaN SMRs grown at various reactor pressures: (a) 100 Torr, (b) 300 Torr, and (c) 500 Torr.

Second, Si impurities diffused from the Si substrate can be substituted for the nearest neighbor of the Ga sites, acting as shallow donors.[25] Figure 3c indicates the CL spectra measured from P1 to P7, as marked on the SEM image in Figure 3a. From P1 to P7, the NBE emission intensity becomes stronger while the YL diminishes, which agrees well with the superimposed monochromatic CL images in Figure 3a. Figure 3d shows the CL spectra measured around the NBE emission peak. The NBE emission peak (3.369 eV) from the lower side of the GaN SMRs shifted by about 28 meV (3.02 nm) from that of the strain-free bulk GaN (3.397 eV) due to the tensile strain on the *a*-axis.[26] The shift for NBE emission peak caused by biaxial strain can be explained by eq 1:[27,28]

$$\Delta E_{NBE} = (2\alpha + \beta q)\varepsilon_{xx} \tag{1}$$

where ΔE_{NBE} is the energy shift of NBE by the biaxial strain, α and β are the constants related to the deformation potentials of both conduction and valence bands, $q = -2C_{13}/C_{33}$ is the ratio of elastic constants, and $\varepsilon_{xx} = (a - a_0)/a_0 = \varepsilon_{yy} = \varepsilon_{zz}/q$ is the *xx*-components of the strain tensor in the hexagonal (wurtzite) symmetry. In general, since $2\alpha + \beta q$ has a negative value from -6 to -12 eV[27,29,] and ε_{xx} is positive in the tensile strained environment, ΔE_{NBE} becomes negative. Therefore, the NBE emission peak was shifted toward lower energy by the tensile strain. As can be seen in Figure 3d, the lower part of the GaN SMR suffers the strong tensile strain, while the tensile strain at the upper part of the SMR is relaxed. To more accurately investigate the magnitude of strain, we conducted TEM measurements on a single GaN SMR at a point 1 μm away from the substrate. The inset of Figure 3b shows the diffraction pattern along the $[11\bar{2}0]$ zone-axis, indicating that the GaN SMR grows along the $\langle 000\bar{1}\rangle$ direction. Figure 3b shows a high resolution lattice image of the GaN SMR. The lattice constants *a* and *c* were measured as 0.327 and 0.513 nm, respectively. We can compare the lattice constants of our GaN SMRs with those of the strain-free GaN (*a*, 0.318 nm; *c*, 0.519 nm) from the literature.[30,31] Therefore, strong tensile strain was applied along the *a*-axis of the GaN SMR, and weak compressive strain was applied along the *c*-axis. The tensile strain on the top $(000\bar{1})$ GaN surface can be explained by the large lattice mismatch between GaN and Si(111) substrates,[20−22] and the compressive strain on the $\{1\bar{1}00\}$ planes can be described by the Poisson effect, which is the phenomenon that the expansion (contraction) occurs in the other directions perpendicular to the direction of applied compression (tensility).[32]

Although the thermodynamic equilibrium shapes of any materials are mainly defined by the surface energies of the crystal planes on these materials, their shapes can also be strongly affected by the changes in adatom diffusion corresponding to the variations in growth conditions, such as the substrate temperature, precursor gas flux, reactor pressure, and V/III molar ratio. Parts a−c of Figure 4 show the 30-deg-tilted SEM images of GaN SMRs grown at various reactor pressures of 100, 300, and 500 Torr for 20 min, respectively. To confirm the relation between the growth rate and the reactor pressure, we changed the reactor pressure inside the chamber while maintaining the other growth conditions, such as the substrate temperature, precursor gas flux, and V/III molar ratio. With increasing reactor pressures from 100 to 500 Torr, the growth rate of the GaN SMRs along the $\langle 000\bar{1}\rangle$ direction dramatically increased from about 2.97 ± 1.21 to 9.86 ± 3.11 μm/h, while the growth rate along the $[1\bar{1}00]$ direction is almost stable at about 2.5 μm/h.

Generally the growth rate V_G in the thin-film model follows eq 2:[33,34]

$$V_G = \frac{kC_i}{1 + Da} = \frac{C_i}{1/k + \delta/D_B} \tag{2}$$

where *k* is the rate constant for the first-order heterogeneous surface reaction, C_i is the inlet concentration of the reactant species at the top of the boundary layer, *Da* is the dimensionless Damköhler number, which is a relative rate of chemical reaction versus diffusive transport, δ is the thickness of the boundary layer, and D_B is the diffusion coefficient through the boundary layer.

The growth rate V_G has the following relation with the reactor pressure by substituting $\delta \propto p^{-1/2}$,[35] $D_B \propto p^{-1}$, and $k = k_{ads} - k_{des} = k_0 p \exp(-E_a/k_B T)$, where k_{ads} is the adsorption rate constant, k_{des} is the desorption rate constant, k_0 is the pre-exponential factors, E_a is the activation energy, and k_B and *T* are the Boltzmann constant and temperature, respectively, into eq 2:

$$V_G \propto \frac{1}{1/k_0 p \exp(-E_a/k_B T) + \sqrt{p}} \tag{3}$$

In eq 3 we defined the reaction rate constant *k* as $k_0 p \exp(-E_a/k_B T)$, which is linearly dependent on the reactor pressure. If the partial pressure near the surface of the substrate increases, the concentration of the Ga adatoms also increases. Thus, the adsorption probability of the Ga adatom increases and the desorption probability decreases due to the increase in the chemical potential of the Ga adatom in the gas phase, which raises the transition probability to the solid phase GaN. This relationship with various pre-exponential factors k_0 in the reaction rate constant *k* is illustrated in Figure 5a. The shape of the curve of the growth rate V_G as a function of the reactor pressure *p* is strongly influenced by the value of k_0. If k_0 has a sufficiently low value, as the reactor pressure increases, so does V_G, as indicated by the blue dashed and dotted line in Figure 5a. On the other hand, if k_0 has a high value, as the reactor pressure increases, the growth rate V_G decreases in an inversely proportional manner to $p^{1/2}$, as represented by a red dashed and dotted dot line in Figure 5a.[36] In general, in the case of 2-

dx.doi.org/10.1021/cg300764f | *Cryst. Growth Des.* 2012, 12, 3838−3844

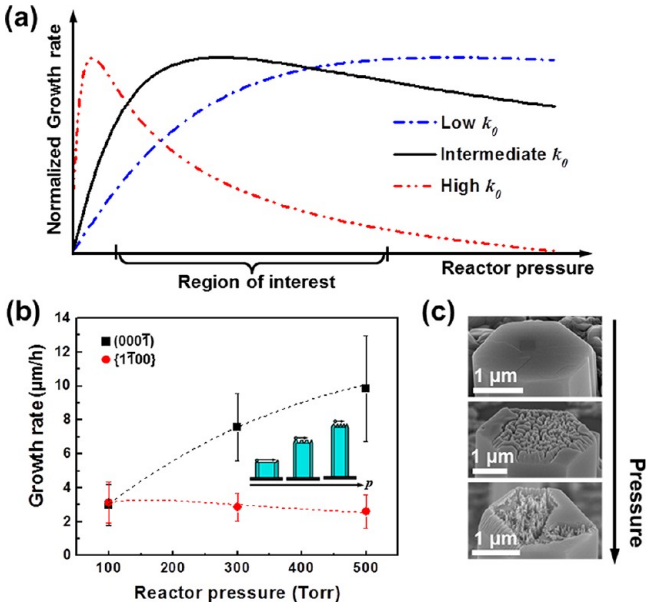

Figure 5. (a) Estimated curves of the growth rate as a function of the reactor pressure with the various pre-exponential factors k_0 in the reaction rate constant k. (b) Measured curve of the growth rates of the GaN SMRs as a function of the reactor pressure along the $\langle 000\bar{1} \rangle$ direction and the $[1\bar{1}00]$ direction. (c) Surface morphology of the top $(000\bar{1})$ GaN surface grown at various reactor pressures.

dimensional (2D) GaN growth with a high V/III molar ratio, the desorption rate decreases due to the high NH_3/H_2 ratio, and consequently, as the difference between k_{ads} and k_{des} increases, so does the value of k_0. On the contrary, in the case of 1-dimensional (1D) GaN growth with a low V/III molar ratio, the desorption rate increases because of the low NH_3/H_2 ratio,[37] and then k_0 has a low value. Figure 5b shows the growth rates of our GaN SMRs on the Si(111) substrate as a function of the reactor pressure along their $\langle 000\bar{1} \rangle$ and the $[1\bar{1}00]$ direction. Since we grew the GaN SMRs on the Si(111) substrate with a low V/III molar ratio for 1D GaN growth, the curve of the growth rate as a function of the reactor pressure in Figure 5b has a similar shape to the blue dashed and dotted line in Figure 5a, as we expected. The growth rate along the $\langle 000\bar{1} \rangle$ direction of the GaN SMRs on the Si(111) substrate increases remarkably as the reactor pressure increases, whereas the growth rate along the $[1\bar{1}00]$ direction of the GaN SMRs on the Si(111) substrate rarely changed due to the huge anisotropy of the activation barriers on the top $(000\bar{1})$ GaN surface and on the $\{1\bar{1}00\}$ GaN sidewalls. The activation energy for the Ga adatom to diffuse into the neighbor sites on the $\{1\bar{1}00\}$ GaN sidewalls (~0.93 eV) is larger by a factor of about 4.65 than that on the top $(000\bar{1})$ GaN surface (~0.2 eV).[38,39] We can, therefore, assume that the effect of the adatom kinetics of Ga adatom on the growth rate along the $[1\bar{1}00]$ direction is negligible. Figure 5c shows SEM images of the top $(000\bar{1})$ GaN surface of the SMRs grown at various reactor pressures. Since the diffusion length λ_d is proportional to $D_S^{1/2} \propto p^{-1/2}$, where D_S is the surface diffusion coefficient, the diffusion length decreases with increasing the reactor pressure. Under low reactor pressure, the probability of a Ga adatom attaching to the edge of the existent terrace is high due to the long surface diffusion length (top of Figure 5c). On the other hand, under high reactor pressure, new 3D GaN islands are well formed by the collisions between the Ga atom and the other particles due to the short surface diffusion length (bottom of Figure 5c). Therefore, the short surface diffusion leads to 3D GaN growth, which is advantageous for vertical growth (1D wire growth), while the long surface diffusion induces 2D GaN growth, which is favorable for the lateral growth (2D thin film growth). Besides the reactor pressure, the V/III molar ratio is also a significant factor in deciding the shape of GaN SMRs. Some research groups have demonstrated that, as the V/III ratio decreases, the aspect ratio of SMRs increases.[40] We could also easily show that the SMRs grown with the low V/III molar ratio have a higher aspect ratio than that grown with the high V/III molar ratio by using eq 3 when the pressure is constant. Thus, under high reactor pressure with a low V/III ratio, we can obtain SMRs with high aspect ratios.

Lastly, we introduce the effect of the biaxial strain on the height of the activation barriers on the top $(000\bar{1})$ GaN surface and on the $\{1\bar{1}00\}$ GaN sidewalls. The biaxial strain applied on

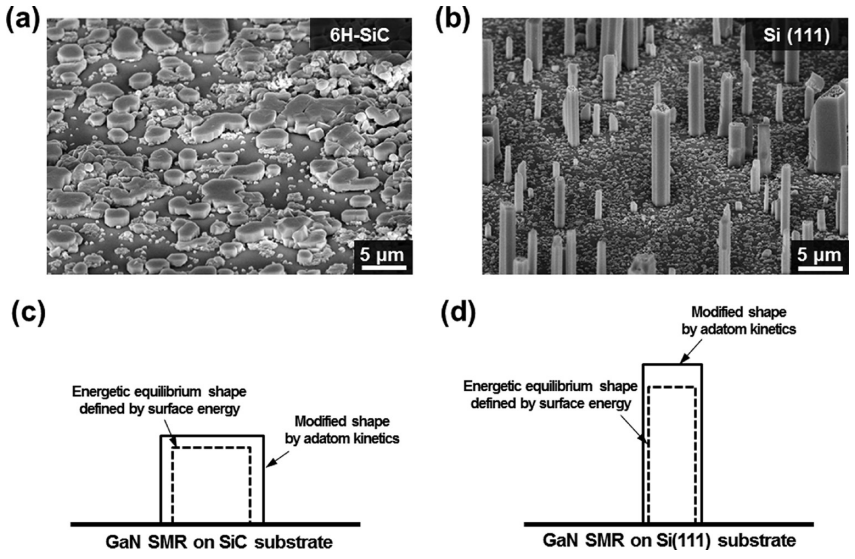

Figure 6. GaN SMRs grown (a) on the 6H-SiC and (b) on the Si(111) substrates at 500 Torr. Growth mechanism of the GaN SMRs (c) on the 6H-SiC and (d) on the Si(111) substrates.

dx.doi.org/10.1021/cg300764f | Cryst. Growth Des. 2012, 12, 3838–3844

the top $(000\bar{1})$ GaN surface not only plays an important role in adjusting the surface energy but also controls the height of the activation barrier for the Ga adatom to diffuse into neighboring sites. Parts a and b of Figure 6 show SEM images of the GaN SMRs grown on the 6H-SiC and the Si(111) substrates at the same time at 500 Torr with a low V/III molar ratio, respectively. The shape of these GaN SMRs is the result of a combination of the effects by the surface energies and the anisotropic activation barriers on the top $(000\bar{1})$ GaN surface and on the $\{1\bar{1}00\}$ GaN sidewalls, and by the changes in the activation barrier due to the biaxial strain applied on their surfaces. The tensile strain on the top $(000\bar{1})$ GaN surface lowers the activation barrier of the Ga adatom, whereas the compressive strain on the top $(000\bar{1})$ GaN surface increases the activation energy of the Ga adatom.[41] Thus, the growth rate of the GaN SMRs on the Si(111) substrate along the $\langle 000\bar{1}\rangle$ direction is much faster than that on the 6H-SiC substrate. Moreover, the compressive strain on the $\{1\bar{1}00\}$ GaN sidewalls of the GaN SMRs on Si(111) substrates reduces the growth rate along the $[1\bar{1}00]$ direction, while the tensile stain on the $\{1\bar{1}00\}$ GaN sidewalls of the GaN SMRs on 6H-SiC substrates enhances the lateral growth of the $\{1\bar{1}00\}$ GaN sidewalls. Therefore, as shown in Figure 6c and d, the GaN SMRs on the Si(111) substrate have a much higher aspect ratio than that on the 6H-SiC substrate by the combination of the effects mentioned above.

To reduce the surface damage on GaN submicrometer- and micrometer-sized structures by dry or wet etching and to raise their quality, the bottom-up growth method is preferred rather than the top-down etching method. However, it is not easy to design the final shape of the GaN submicrometer- and micrometer-sized structures without an exact estimation based on the DFT calculation and consideration of the adatom kinetics. In these regards, our approaches proposed in this paper could play an important role as a guideline to predict the final shape of GaN submicrometer- and micrometer-sized structures.

4. CONCLUSION

We have successfully grown vertically well-aligned GaN SMRs on Si(111) substrates without the use of catalysts, patterning processes, or doping constituents. Based on our DFT simulation and the comparative experimental results, we found that the tensile strain on the top $(000\bar{1})$ surface increases the surface energy of the $(000\bar{1})$ GaN surface and, hence, the vertical growth rate of GaN SMRs. The magnitude and direction of the tensile strain along the GaN SMRs were confirmed by the CL and TEM measurements. We have also verified that a high reactor pressure results in a high growth rate at a low V/III ratio. In addition, the growth rate of a certain plane was greatly influenced by the activation energy for the Ga adatom to bind into the surface and the variation of chemical potential and surface diffusion of the Ga adatom.

■ ASSOCIATED CONTENT

Supporting Information

All details of the methodologies and the atomic structures for the calculation of the surface energy with DFT simulations, the top $(000\bar{1})$ surface confirmation test results by the chemical wet etching with 12 M KOH solution, and additional information. This material is available free of charge via the Internet at http://pubs.acs.org.

■ AUTHOR INFORMATION

Corresponding Author

*E-mail: yhc@kaist.ac.kr. Tel: +82-10-2058-6407. Fax: +82-42-350-5549.

Notes

The authors declare no competing financial interest.

■ ACKNOWLEDGMENTS

This work was supported by a WCU Program (No. R31-2008-000-1071-0) of the Ministry of Education, Science and Technology, and by the KAIST EEWS Initiative.

■ REFERENCES

(1) Hersee, S. D.; Fairchild, M.; Rishinaramangalam, A. K.; Ferdous, M. S.; Zhang, L.; Varangis, P. M.; Swartzentruber, B. S.; Talin, A. A. *Electron. Lett.* **2009**, *45*, 75−76.
(2) Guo, W.; Zhang, M.; Banerjee, A.; Bhattacharya, P. *Nano Lett.* **2010**, *10*, 3355−3359.
(3) Johnson, J. C.; Choi, H.; Knutsen, K. P; Schaller, R. D.; Yang, P.; Saykally, R. J. *Nat. Mater.* **2002**, *1*, 106−110.
(4) Greytak, A. B.; Barrelet, C. J.; Li, Y.; Lieber, C. M. *Appl. Phys. Lett.* **2005**, *87*, 151103−151105.
(5) Park, C. Y.; Lim, J. M.; Yu, J. S.; Lee, Y. T. *Appl. Phys. Lett.* **2010**, *96*, 151909−151911.
(6) Burke, R. A.; Lamborn, D. R.; Weng, X.; Redwing, J. M. *J. Cryst. Growth* **2009**, *311*, 3409−3416.
(7) Mastro, M. A.; Freitas, J. A., Jr.; Twigg, M.; Holm, R. T.; Eddy, C. R., Jr.; Kub, F.; Kim, H. Y.; Ahn, J.; Kim, J. *Phys. Status Solidi A* **2008**, *205*, 378−382.
(8) Bergbauer, W.; Strassburg, M.; Kölper, C.; Linder, N.; Roder, C.; Lähnemann, J.; Trampert, A.; Fündling, S.; Li, S. F.; Wehmann, H. H.; Waag, A. *J. Cryst. Growth* **2011**, *315*, 164−167.
(9) Hersee, S. D.; Sun, X.; Wang, X. *Nano Lett.* **2006**, *6*, 1808−1811.
(10) Kuo, S. Y.; Lai, F. I.; Chen, W. C.; Hsiao, C. N. *J. Cryst. Growth* **2008**, *310*, 5129−5133.
(11) Vajpeyi, A. P.; Georgakilas, A.; Tsiakatouras, G.; Tsagaraki, K.; Androulidaki, M.; Chua, S. J.; Tripathy, S. *Physica E* **2009**, *41*, 427−430.
(12) Kwon, Y. H.; Lee, K. H.; Ryu, S. Y.; Kang, T. W.; You, C. H.; Kim, T. W. *Appl. Surf. Sci.* **2008**, *254*, 7014−7017.
(13) Kresse, G; Furthmüller, J. *Comput. Mater. Sci.* **1996**, *6*, 15−50.
(14) Blöchl, P. *Phys. Rev. B* **1994**, *50*, 17953−17979.
(15) Perdew, J. P; Burke, K; Ernzerhof, M. *Phys. Rev. Lett.* **1996**, *77*, 3865−3868.
(16) Keating, C. D.; Natan, M. J. *Adv. Mater.* **2003**, *15*, 451−454.
(17) Du, D.; Srolovitz, D. J.; Coltrin, M. E.; Mitchell, C. C. *Phys. Rev. Lett.* **2005**, *95*, 155503−155506.
(18) Northrup, J. E.; Neugebauer, J. *Phys. Rev. B* **1996**, *53*, R10477−R10480−R10483.
(19) Chen, X. J.; Perillat-Merceroz, G.; Sam-Giao, D.; Durand, C.; Eymery, J. *Appl. Phys. Lett.* **2010**, *97*, 151909−151911.
(20) Matsumura, S.; Inushima, T.; Shiraishi, T. *J. Cryst. Growth* **1998**, *189/190*, 696−700.
(21) Roder, C.; Einfeldt, S.; Figge, S.; Hommel, D. *Phys. Rev. B* **2005**, *72*, 085218−085223.
(22) Slack, G. A.; Bartram, S. F. *J. Appl. Phys.* **1975**, *46*, 89−98.
(23) Zamir, S.; Meyler, B.; Zolotoyabko, E.; Salzman, J. *J. Cryst. Growth* **2000**, *218*, 181−190.
(24) Dadgar, A.; Veit, P.; Schulze, F.; Bläsing, J.; Krtschil, A.; Witte, H.; Diez, A.; Hempel, T.; Christen, J.; Clos, R.; Krost, A. *Thin Solid Films* **2007**, *515*, 4356−4361.
(25) Arslan, E.; Duygulu, Ö.; Kaya, A. A.; Teke, A.; Özçelik, S.; Ozbay, E. *Superlattices Microstruct.* **2009**, *46*, 846−857.
(26) Chichibu, S.; Azuhata, T.; Sota, T.; Amano, H.; Akasaki, I. *Appl. Phys. Lett.* **1997**, *70*, 2085−2087.

(27) Davydov, V. Y.; Averkiev, N. S.; Goncharuk, I. N.; Nelson, D. K.; Nikitina, I. P.; Polkovnikov, A. S.; Smirnov, A. N.; Jacobson, M. A.; Semchinova, O. K. *J. Appl. Phys.* **1997**, *82*, 5097−5102.
(28) Shikanai, A.; Azuhata, T.; Sota, T.; Chichibu, S.; Kuramata, A.; Horino, K.; Nakamura, S. *J. Appl. Phys.* **1997**, *81*, 417−424.
(29) Shan., W.; Hauenstein, R. J.; Fischer, A. J.; Song, J. J.; Perry, W. G.; Bremser, M. D.; Davis, R. F.; Goldenberg, B. *Phys. Rev. B* **1996**, *54*, 13460−13463.
(30) Lahrèche, H.; Vennéguès, P.; Tottereau, O.; Laügt, M.; Lorenzini, P.; Leroux, M.; Beaumont, B.; Gibart, P. *J. Cryst. Growth* **2000**, *217*, 13−25.
(31) Porowski, S. *J. Cryst. Growth* **1998**, *189/190*, 153−158.
(32) Moram, M. A.; Barber, Z. H.; Humphreys, C. J. *J. Appl. Phys.* **2007**, *102*, 023505−023508.
(33) Du, D; Srolovitz, D. J. *J. Cryst. Growth* **2006**, *296*, 86−96.
(34) Coltrin, M. E.; Mitchell, C. C. *J. Cryst. Growth* **2003**, *254*, 34−45.
(35) Shibata, N.; Zembutsu, S. *Jpn. J. Appl. Phys.* **1987**, *26*, 1416−1421.
(36) Dauelsberg, M.; Martin, C.; Protzmann, H.; Boyd, A. R.; Thrush, E. J.; Käppeler, J.; Heuken, M.; Talalaev, R. A.; Yakovlev, E. V.; Kondratyev, A. V. *J. Cryst. Growth* **2007**, *298*, 418−424.
(37) Koleske, D. D.; Wickenden, A. E.; Henry, R. L.; Culbertson, J. C.; Twigg, M. E. *J. Cryst. Growth* **2001**, *223*, 466−483.
(38) Jindal, V.; Shahedipour-Sandvik, F. *J. Appl. Phys.* **2010**, *107*, 054907−054912.
(39) Lymperakis, L.; Neugebauer, J. *Phys. Rev. B* **2009**, *79*, 241308(R)−241311(R).
(40) Koester, R.; Hwang, J. S.; Durand, C.; Le Si Dang, D.; Eymery, J. *Nanotechnology* **2010**, *21*, 015602−015610.
(41) Grandusky, J. R.; Jindal, V.; Raynolds, J. E.; Guha, S.; Shahedipour-Sandvik, F. *Mater. Sci. Eng., B* **2009**, *158*, 13−18.